JEE Journal of Ecological Engineering

Journal of Ecological Engineering, 2027, 28(1), 389–412
https://doi.org/10.12911/22998993/242649
ISSN 2299–8993, License CC-BY 4.0

Received: 2026.08.30
Accepted: 2026.11.16
Published: 2026.12.01

Waste lubricating oil pyrolysis over copper-modified fluid catalytic cracking catalyst for hydrocarbon fuel: An optimization and integrated process simulation

Didi Dwi Anggoro[1*], Eko Santoso[2], Didik Prasetyoko[2], Aishah Abdul Jalil[3], Taufiq-Yap Yun Hin[4], Akmal Athalah[1], Fauzi Sufyan[1], Brilliant Umara Le Monde[1], Jhilena Abigail Luberzky Sinuraya[1]

[1] Department of Chemical Engineering, Faculty of Engineering, Diponegoro University, Tembalang, Semarang, Central Java, 50275, Indonesia
[2] Department of Chemistry, Faculty of Science and Data Analytics, Institut Teknologi Sepuluh Nopember (ITS), Sukolilo, Surabaya, 60111, Indonesia
[3] Faculty of Chemical and Energy Engineering, Universiti Teknologi Malaysia, 81310, UTM Johor Bahru, Johor, Malaysia
[4] Catalysis Science and Technology Research Centre (PutraCat), Faculty of Science, Universiti Putra Malaysia, 43400 UPM Serdang, Selangor, Malaysia
* Corresponding author's e-mail: anggorophd@gmail.com

ABSTRACT

This study investigates the catalytic pyrolysis of waste lubricating oil using a copper-modified fluid catalytic cracking catalyst (Cu/FCC) for the production of diesel-range hydrocarbon fuel. The influence of catalyst loading (1–3% w/v) and reaction time (60–180 min) on liquid fuel yield was evaluated through response surface methodology (RSM) based on central composite design (CCD). The liquid yield ranged from 79.22 to 90.00%, The corrected quadratic model was statistically significant (R^2 = 0.9712) and predicted an optimum liquid yield of approximately 89.37% at a catalyst loading of 2.92% (w/v) and a reaction time of 79.81 min. GC-MS analysis indicated that the condensable product was dominated by higher-molecular-weight hydrocarbons, particularly compounds within the C16-C21 range, while process simulation using Aspen HYSYS supported the predominance of condensable hydrocarbon fractions under the modeled operating conditions. Catalyst characterization confirmed successful Cu incorporation, with the Cu content increasing from 0.0074 wt% in FCC to 0.689 wt% in Cu/FCC. NH_3-TPD showed that the total acidity decreased from 2.899 mmol NH_3 g^{-1} for FCC to 1.343 mmol NH_3 g^{-1}after Cu modification. BET and XRD analyses indicated that Cu impregnation moderately altered the catalyst texture while largely preserving the FCC crystalline framework. Cu-modified FCC shows potential for the catalytic conversion of WLO into liquid hydrocarbons enriched in diesel-range components.

Keywords: waste lubricant oil, diesel, catalyst, Cu/FCC, optimization.

INTRODUCTION

The continuous growth of population, urbanization, and economic activity has contributed to increasing energy and fuel consumption, particularly in rapidly developing countries such as Indonesia (Muzayanah et al., 2022; Naz et al., 2014). Indonesia's population increased from approximately 237.6 million in 2010 to 281.6 million in 2024. During the same period, the number of motor vehicles increased substantially, reaching approximately 105.3 million units in 2015 and about 149.7 million units in 2022 (Dewi et al., 2022). The rapid expansion of vehicular transportation has consequently increased the demand for automotive lubricants and, in turn, the generation

of waste lubricating oil. Globally, the lubricant market was valued at approximately USD 157.6 billion and was projected to reach USD 182.6 billion by 2025, with automotive lubricants accounting for approximately 57% of total lubricant demand (Mishra et al., 2021).

Lubricating oils play a critical role in reducing friction and wear between moving mechanical components while simultaneously contributing to cooling, corrosion protection, sealing, and contaminant removal during engine operation. Commercial lubricants are generally formulated from a base oil combined with functional additives, including antioxidants, detergents, dispersants, anti-wear agents, corrosion inhibitors, and viscosity modifiers. Depending on the lubricant formulation, additives may constitute up to approximately 20 wt% of the finished product (Musadi et al., 2024; Nasim et al., 2014) However, lubricating oils progressively deteriorate as a result of thermal and oxidative degradation, additive depletion, fuel dilution, water contamination, combustion-derived particulates, and the accumulation of metallic wear debris. Consequently, the oil gradually loses its original physicochemical and tribological performance and must eventually be replaced, thereby generating waste lubricating oil (WLO).

Used lubricating oil represents a significant hazardous hydrocarbon waste because it contains degraded hydrocarbons, residual additives, oxidation products, metals, and other organic and inorganic contaminants (Singh et al., 2025). emphasized that improperly managed WLO can pose substantial risks to human health and the environment, particularly when released into soil or water systems. Approximately half of fresh lubricating oil may ultimately become collectable used oil, while the remaining fraction is lost during service through combustion, evaporation, leakage, and residues retained in equipment or containers (Moses et al., 2023)

Improper disposal of used lubricating oil can severely affect terrestrial and aquatic environments. Petroleum hydrocarbons and associated contaminants can alter soil physicochemical properties, reduce biological activity, and contaminate surface and groundwater systems. Hydrophobic oil films can also interfere with oxygen transfer at the air-water interface and adversely affect aquatic organisms. The environmental persistence of lubricating oils is particularly concerning because even relatively small quantities may contaminate substantial volumes of water. (Nowak et al., 2019) reported that one liter of petroleum-derived lubricating oil may render up to approximately one million liters of drinking water unsuitable for consumption. Therefore, uncontrolled disposal of waste lubricating oil represents both a resource loss and a potentially serious environmental burden.

Global recovery of used lubricating oil also remains incomplete. Historical estimates indicate that approximately 42 million tonnes of lubricating oil were consumed worldwide annually, of which only around 20 million tonnes were systematically collected as used oil (Botas et al., 2017). More recent assessments also reveal considerable regional differences in collection and regeneration rates. The average waste-oil collection rate in the European Union has been reported at approximately 82%, whereas substantial quantities remain unaccounted for in several other regions (European Commission, 2021). These differences highlight the continued need for technologies capable of converting used lubricating oil into value-added products rather than relying on disposal or uncontrolled combustion.

Although pyrolysis has been widely studied for plastic and tire waste, research focusing on used lubricating oil remains relatively limited. Previous studies have demonstrated that catalytic pyrolysis can significantly improve oil yield, with reported values ranging from below 20% to above 90% depending on catalyst type and operating conditions. In particular, FCC-based catalysts have shown promising performance due to their high activity and selectivity. Catalyst modification with transition metals provides an additional strategy for tuning catalytic activity and product selectivity. Metal incorporation can modify catalyst acidity, pore accessibility, and the distribution of active sites. Among the transition metals investigated for hydrocarbon conversion, Cu is particularly interesting because its incorporation into FCC-type materials can alter acid-site characteristics and affect the cracking and secondary transformation of hydrocarbons. (Charusiri et al., 2023) investigated Cu-modified spent FCC catalyst for lubricating oil conversion and demonstrated the influence of copper modification on catalyst acidity and hydrocarbon product distribution. However, the use of spent FCC catalyst may introduce uncertainties associated with previous refinery operation, including coke deposition, metal contamination, and variation in surface properties.

In contrast, the present study employs a fresh FCC catalyst modified with Cu, providing a controlled platform to evaluate the intrinsic effect of Cu incorporation on catalytic performance.

Fresh commercial FCC was used as the starting support rather than spent FCC, allowing the effect of Cu incorporation to be evaluated without the confounding influence of previous refinery exposure, coke deposition, accumulated metals, or prior catalyst deactivation. The present work investigates waste lubricating oil as the sole hydrocarbon feed rather than co-pyrolysis with plastic. Catalyst loading and reaction time were systematically optimized using Response Surface Methodology based on a Central Composite Design, enabling evaluation of linear, interaction, and quadratic effects on condensable liquid yield. In Cu-modified FCC systems, insufficient metal loading may provide only limited modification of catalytic activity, whereas excessive metal incorporation can cover active sites, block pores, or promote secondary reactions that decrease the yield of desirable condensable hydrocarbons. In addition to catalyst development, systematic optimization of operating conditions is required because pyrolysis responses are generally nonlinear and result from interactions among several process variables. Response surface methodology (RSM) provides a statistically efficient framework for evaluating these interactions and identifying optimum operating regions with a relatively limited number of experiments. Central composite design (CCD), one of the most widely applied RSM designs, enables the development of quadratic models that can describe linear, interaction, and curvature effects. Recent pyrolysis studies have successfully employed RSM-CCD to optimize factors such as temperature, residence time, and heating rate for maximizing liquid yield and minimizing solid residue (Boro and Tiwari, 2025). Recent studies have demonstrated that advanced optimization strategies are valuable tools for improving renewable fuel conversion performance and identifying favorable operating parameters in complex energy systems (Al-jabiri et al., 2024)

Furthermore, integrated process simulation has become increasingly important for evaluating the feasibility of sustainable energy conversion technologies. Simulation approaches enable the analysis of process behavior, material flow, energy performance, and potential scale-up considerations beyond experimental evaluation alone. Previous studies have demonstrated that system-level modeling and simulation can provide comprehensive insights into the performance and optimization of advanced energy systems (Al-Rbaihat, 2025). Similar approaches are increasingly relevant for catalytic fuel production systems where experimental performance must be connected with process-level evaluation.like liquid fuel or fuel precursor.

MATERIALS AND METHODS

Materials

Waste lubricating oil used as feedstock was collected from local motor vehicle service facilities. Prior to use, the oil was filtered to remove suspended solids and impurities. A commercial fluid catalytic cracking (FCC) catalyst obtained from the Pertamina Balongan Refinery was used as the catalyst support. Copper nitrate hydrate ($Cu(NO_3)_3.2.5H_2O$) Merck was employed as the metal precursor for catalyst modification.

Catalyst preparation

The Cu-impregnated FCC catalyst was prepared via the wet impregnation method, with the preparation procedure illustrated in Figure S1 of the Supplementary Information. Initially, 40 g of FCC catalyst was mixed with an aqueous solution containing 5 wt% $Cu(NO_3)_2 \cdot 2.5H_2O$ dissolved in 100 mL of distilled water. The mixture was stirred at 250 rpm and heated at 80 °C until a homogeneous slurry was formed. The resulting slurry was dried in an oven at 110 °C for 12 h to remove moisture, followed by calcination in a furnace at 450 °C for 3 h to obtain the active Cu/FCC catalyst. The prepared catalyst was subsequently characterized to evaluate its physicochemical properties.

Catalyst characterization

The physicochemical properties of the prepared catalyst were analyzed using several techniques. The crystalline structure and phase characteristics of the catalysts were investigated using wide-angle X-ray diffraction (XRD). The XRD measurements were performed using a PANalytical X'Pert MPD diffractometer equipped with Cu-Kα radiation (λ = 1.5406 Å). The diffraction patterns were recorded over a 2θ range of 5–80°

with a scanning rate of 2° min^{-1} under ambient conditions. The obtained diffraction patterns were analyzed to identify the crystalline phases present in the FCC-based catalysts and to evaluate structural changes after Cu modification and catalytic reaction. Phase identification was performed by comparing the experimental diffraction peaks with reference patterns from the International Centre for Diffraction Data (ICDD) database.

$$n\lambda = 2d \sin \quad (1)$$

$$d = \frac{n\lambda}{2 \sin \theta} \quad (2)$$

$$I_c(\%) = \frac{A_c}{A_c + A_a} \times 100 \quad (3)$$

The elemental composition of the catalysts was determined using X-ray fluorescence (XRF) analysis. The measurements were performed using a Rigaku X-ray fluorescence spectrometer equipped with powder sample analysis capability. The catalyst samples were prepared as powder samples and analyzed using a pressed powder configuration. Approximately 4.3900 g of catalyst sample was prepared for measurement with a sample diameter of 30.0 mm and thickness of approximately 3.0 mm.

The textural properties of the catalyst samples were characterized by nitrogen (N_2) adsorption desorption analysis at approximately 77 K using a Micromeritics TriStar II series surface area and porosity analyzer. The specific surface area (S_{BET}) was determined using the Brunauer-Emmett-Teller (BET) method. The pore-size distribution (PSD), cumulative pore volume (V_{BJH}), and average pore diameter (D_{BJH}) were calculated using the Barrett-Joyner-Halenda (BJH) method based on the desorption branch of the N_2 isotherms.

The acidity of the catalyst was characterized by ammonia temperature-programmed desorption (NH_3-TPD) using a Thermo TPD/R/O 1100 analyzer. Approximately 0.05 g of catalyst was subjected to pretreatment under nitrogen flow before NH_3-TPD analysis. During the desorption step, helium was used as the carrier gas at a flow rate of 20 mL min^{-1}. The temperature was increased from 50 to 700 °C at a heating rate of 20 °C min^{-1} and subsequently held at 700 °C for 30 min. The amount of desorbed ammonia was quantified to determine the total acidity and the distribution of acid-site strengths of the catalyst. Following the NH_3 adsorption step, physically adsorbed ammonia was removed under flowing inert gas before initiating the programmed desorption measurement. The NH_3-TPD analysis was subsequently performed under helium as the carrier gas at a flow rate of 20 mL min^{-1}. The desorption program was initiated at 50 °C, after which the temperature was increased to 700 °C at a heating rate of 20 °C min^{-1}. The final temperature of 700 °C was maintained for 30 min to ensure desorption of strongly adsorbed ammonia species. Quantitative acidity was determined by integration of the NH_3 desorption peak after baseline correction using the instrument calibration factor.

Thermogravimetric analysis (TGA) was conducted to evaluate the thermal behavior of the fresh and spent catalysts. TGA measurements were performed under an inert nitrogen atmosphere. Prior to programmed heating, the analysis chamber was purged with N_2 at a flow rate of 20 mL min^{-1} for 10 min to remove residual air. The sample was subsequently maintained at 100 °C for 10 min to remove physically adsorbed moisture, after which the temperature was increased to 800 °C at a constant heating rate of 20 °C min^{-1}.

Setup and pyrolysis procedure

Catalytic pyrolysis experiments were conducted using a laboratory-scale batch pyrolysis reactor equipped with a fixed catalytic bed in the vapor pathway and a two-stage condensation system, as illustrated in Figure 1. The reactor chamber was fabricated from stainless steel SS 304 with a wall thickness of 5 mm. The experimental system consisted of a reactor chamber, a waste lubricating oil feed inlet, a catalyst holder, temperature-monitoring probes, a pressure gauge, a vapor/product outlet line, and two condensers connected in series, as illustrated in Figure S2 of the Supplementary Information.

Experimental design

A CCD with two independent variables at five coded levels was generated using Statistica 6.0. The investigated factors were catalyst loading (X_1, % w/v) and reaction time (X_2, min). The CCD consisted of 10 experimental runs, including four factorial points, four axial points, and two replicated center points. For the two-factor rotatable design, the axial distance was $\alpha = 1.4142$. The corresponding catalyst-loading levels were 0.5858, 1.0000, 2.0000, 3.0000, and 3.4142% (w/v), while the reaction-time levels were 35.147,



Figure 1. Pyrolysis setup equipment: 1) temperature gauge, 2) inlet oil, 3) pressure gauge, 4) catalyst holder, 5) condenser 1, 6) condenser 2, 7) outlet product gases, 8) outlet product 2, 9) outlet product 1, 10) outlet residue

60.000, 120.000, 180.000, and 204.853 min (Table 1). The center-point replicates were used to estimate pure experimental error. Liquid yield was used as the response variable for quadratic RSM analysis, and statistical significance was evaluated at $p < 0.05$.

Liquid yield and chemical composition

The liquid yield was calculated based on the mass ratio of liquid product to initial feedstock using Equation :

$$Y_{liquid} = \frac{M_1}{M_2} \times 100\% \quad (4)$$

$$Y_{Residue} = \frac{M_3}{M_2} \times 100\% \quad (5)$$

$$Y_{Gas} = 100 - (Y_{liquid} + Y_{Residue}) \quad (6)$$

where: Y_{liquid} is the liquid yield (%), M_1 is the mass of liquid product (g), M_2 is the mass of initial waste oil feed (g), M_3 is mass of residue.

The organic compounds present in the liquid products obtained from the catalytic pyrolysis reaction were analyzed using gas chromatography-mass spectrometry (GC-MS, QP2010 SE, Shimadzu) equipped with an RTX-5MS capillary column (30 m × 0.25 mm internal diameter × 0.25 µm film thickness). Prior to analysis, 2 µL of the liquid product was diluted in 1 mL of GC-grade n-hexane. Subsequently, 1 µL of the diluted sample was injected into the GC-MS system for hydrocarbon composition analysis.

The higher heating value (HHV) of the liquid pyrolysis products was determined using an automatic isoperibol bomb calorimeter (Parr Instrument Model 6400, USA) following the standard combustion calorimetry procedure. This parameter was used to evaluate the energy potential of the pyrolysis oil as an alternative fuel.

Statistical analysis

The experimental data were analyzed using Statistica 6.0. A second-order polynomial equation (Eq. 1) was fitted to the response data:

$$Y = \beta_0 + \sum_{i=1}^{3} \beta_i X_i + \sum_{i=1}^{3} \beta_{ii} X_i^2 + \sum_{i<j} \beta_{ij} X_i X_j \quad (7)$$

where: Y is the predicted response; β_0 is the intercept coefficient; β_i, β_{ii}, and β_{ij} are the linear, quadratic, and interaction coefficients, respectively; and X_i and X_j are the coded independent variables.

The significance of the models and individual regression coefficients was assessed using analysis of variance (ANOVA) at a 95% confidence level ($p < 0.05$). The coefficient of determination (R^2) and the adjusted R^2 were used to evaluate the

goodness-of-fit of the models. Response surface and contour plots were generated to visualize the effects of variable interactions on the responses.

RESULTS AND DISCUSSION

Physicochemical properties of catalyst

The elemental composition of the FCC catalyst was analyzed using X-ray fluorescence (XRF) to evaluate the effect of Cu impregnation on the overall catalyst composition. XRF was selected because it enables rapid, accurate, and non-destructive elemental analysis. The results provide insight into changes in the elemental and metal composition of the catalyst following the impregnation treatment and are summarized in Table S1 of the Supplementary Information. The FCC catalyst was dominated by Al and Si, with concentrations of 14.20 and 9.63%, respectively. Commercial FCC catalysts are multicomponent materials in which zeolite Y provides a major fraction of the cracking activity, while alumina and silica-containing matrices contribute additional textural and catalytic functionality. The significant compositional change following impregnation was observed for Cu. The concentration increased from only 0.0074% in FCC to 0.689% in Cu/FCC. This marked increase provides strong bulk-compositional evidence that Cu was successfully incorporated into the FCC material during impregnation. A similar approach has been reported by (Charusiri et al., 2023), Cu incorporation into spent FCC after wet impregnation and observed measurable Cu loading in the modified catalyst. Similarly, changes in minor elements should be interpreted cautiously. In particular, Y increased from 0.298 to 2.17%, although no Y-containing precursor was introduced during Cu impregnation.

The preparation conditions used during wet impregnation can influence the final distribution and accessibility of supported metal species within porous catalyst supports. (Pereira et al., 2024) demonstrated that wet impregnation is an effective method for incorporating Ni and Cu species into mesoporous supports and that metal loading influences the resulting catalyst properties and catalytic performance. Similarly, (Song et al., 2018) showed that the dispersion of Cu-containing species and suppression of metal aggregation are important factors governing the physicochemical properties of wet-impregnated catalysts. Therefore, the relatively low measured Cu content and the observed textural changes in the present Cu/FCC catalyst may reflect not only the nominal precursor loading but also the distribution, retention, and dispersion of Cu species within the heterogeneous FCC support. Relative reduction is primarily attributed to a dilution effect induced by the addition of the copper precursor into the catalyst mass, rather than the destruction of the structural framework. Furthermore, the measured copper concentration highlights the intricate dynamics of the wet impregnation method. Factors such as the rapid rate of solvent evaporation and capillary forces during the drying phase can dictate the final metal dispersion, potentially leading to localized copper accumulation on certain active sites of the catalyst surface (Liu et al., 2008; Lu et al., 2020).

As shown in Figure 2, the catalysts retained the characteristic diffraction pattern associated with the faujasite-type zeolitic structure of FCC. Typical Y-zeolite-containing FCC catalysts exhibit characteristic reflections in the low- and intermediate-angle regions, including peaks around $2\theta = 6°$, 10°, 15–16°, and 23–25°

The similarity between the diffraction profiles of FCC and fresh Cu/FCC suggests that Cu impregnation did not substantially destroy the original faujasite framework. This finding agrees closely with (Charusiri et al., 2023; Ćurković et al., 1997), who reported characteristic FCC reflections at 2θ values of approximately 6.23°, 10.16°, 15.64°, 23.64°, 27.04°, and 31.38° and observed no major structural change following low-level Cu impregnation of spent FCC.

Table 1. Coded and actual levels of independent variables in the CCD

Independent Variables	Symbol	Values				
		-α (-1.4142)	-1	0	+1	+α (+1.4142)
Catalyst loading (% w/v)	X_1	0.5858	1.00	2.00	3.00	3.4142
Reaction time (min)	X_2	35.147	60.00	120.00	180.00	204.853

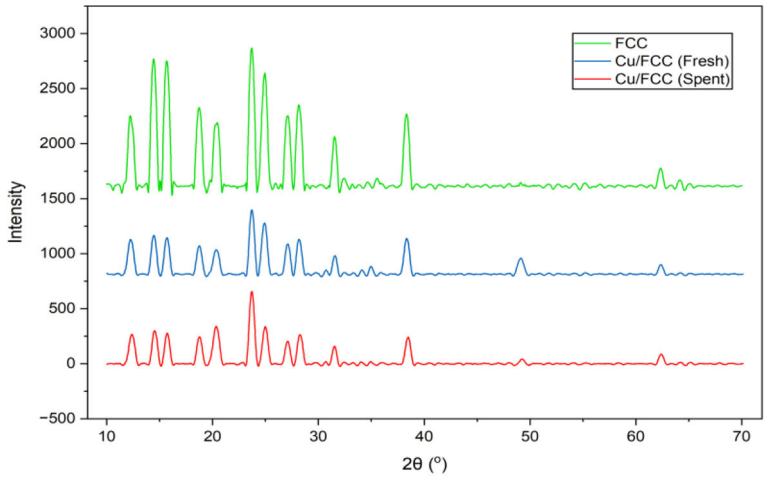

Figure 2. XRD analysis of the catalysts

Table 2. Textural properties of FCC and Cu/FCC catalysts

Catalyst	Crystallinity (%)
FCC	70.55
Cu/FCC (fresh)	69.70
Cu/FCC (spent)	66.90

After Catalytic Pyrolysis, crystallinity decreased further to 66.90% (Table 2), corresponding to an approximately 5.2% reduction relative to the original FCC. Such a moderate decline may arise from a combination of thermal exposure, carbonaceous deposition, and partial structural alteration during catalytic operation. Studies of industrial FCC catalysts have demonstrated that repeated cracking and regeneration can reduce micropore volume and damage crystalline structure, while coke deposition simultaneously contributes to pore blockage and catalyst deactivation (Almas et al., 2019). The spent Cu/FCC maintained 66.90% relative crystallinity, suggesting that a substantial fraction of the zeolitic structure remained intact after reaction. This structural retention is consistent with the known hydrothermal stability of rare-earth-stabilized Y-type FCC catalysts. Rare-earth species, particularly La, can interact with zeolite framework oxygen atoms and increase the structural stability of Y zeolite under severe operating conditions (Zang et al., 2023).

NH_3-TPD analysis showed that Cu modification substantially altered the acidity characteristics of the FCC catalyst. The parent FCC exhibited a total acidity of 2.899 mmol NH_3 g^{-1}, whereas Cu/FCC showed a lower value of 1.343 mmol NH_3 g^{-1}, corresponding to an approximately 53.7% decrease in total NH_3 uptake (Table 3). In addition to the decrease in total acidity, a clear change in the desorption-temperature distribution was observed. The FCC catalyst exhibited desorption features at approximately 178 and 446 °C, with the high-temperature peak accounting for the dominant fraction of NH_3 desorption, whereas Cu/FCC displayed a principal desorption region centered at approximately 373 °C. These results indicate that Cu impregnation modified not only the number of NH_3-accessible acid sites but also their relative strength distribution.

The shift of the dominant desorption region from approximately 446 °C for FCC to 373 °C for Cu/FCC suggests a decrease in the relative contribution of the strongest NH_3-binding sites and a redistribution toward sites of comparatively intermediate strength. Such a change does not necessarily imply deterioration of catalytic performance. (Pan et al., 2018) reported that FCC-type catalysts possessing fewer strong acid sites and a larger contribution of weaker acid sites exhibited favorable heavy-oil conversion together with improved coke selectivity. This demonstrates that catalytic cracking performance is governed by the distribution and accessibility of acid sites rather than by total acidity This improved stability suggests that Cu impregnation mitigates catalyst deactivation by modifying coke formation pathways, resulting in lighter and more easily removable carbon deposits. Consequently, Cu/FCC demonstrates superior resistance to deactivation. The present result differs from the observations of (Charusiri et al., 2023) who reported that Cu loading on spent FCC increased catalyst acidity and contributed to improved catalytic activity

Table 3. NH_3-TPD acidity characteristics of catalysts

Catalyst	Acidity (mmol/g)
FCC	2.899
Cu/FCC	1.343

during the copyrolysis of spent lubricating oil and polyethylene. The acidity resulting from metal modification therefore depends on the initial state of the FCC support, metal loading, metal dispersion, ion-exchange behavior, interaction between the metal species and aluminosilicate framework, and accessibility of the acid sites. The decrease in NH_3 uptake observed in the present Cu/FCC catalyst is also consistent with the accompanying physicochemical characterization. XRF analysis confirmed successful Cu incorporation, with the Cu concentration increasing from 0.0074 to 0.689 wt%, whereas the BET surface area decreased only moderately from 259.343 to 242.187 m^2 g^{-1}. Furthermore, XRD showed only a small decrease in crystallinity from 70.55 to 69.70%. These observations indicate that the decrease in measured acidity is unlikely to originate from extensive destruction of the FCC framework. Instead, the results are more consistent with modification of the accessible acid-site environment following Cu incorporation, potentially through interaction of Cu-containing species with framework-associated acid sites and partial occupation or coverage of sites accessible to NH_3. XRF analysis confirmed in Cu content from 0.0074 to 0.689%, providing direct evidence for successful metal incorporation. Meanwhile, the relatively small reduction in crystallinity from 70.55 to 69.70% indicates that impregnation did not substantially disrupt the original FCC crystalline structure. Similar preservation of the faujasite structure following Cu modification has been reported for Cu-modified spent FCC catalysts. More importantly, Cu modification decreased the measured catalyst acidity from 2.899 to 1.343 mmol g^{-1}, corresponding to an approximately 19% increase. Since hydrocarbon cracking over FCC catalysts is strongly associated with accessible acid sites, this increased acidity provides a plausible explanation for the improved liquid-product yield observed experimentally with Cu/FCC. However, Cu/FCC retained approximately 32.7% of its acidity, compared with only 17.8% for FCC.The spent Cu/FCC maintained a relative crystallinity of 66.90%, indicating that the majority of its crystalline zeolitic structure remained after pyrolysis.

The textural properties of the fresh and spent FCC-based catalysts were evaluated by N_2 adsorption-desorption analysis. Fresh FCC exhibited a BET surface area of 259.343 m^2 g^{-1}, a total pore volume of 0.1903 cm^3 g^{-1}, and an average pore diameter of 2.935 nm (Table 4). Following Cu impregnation, the BET surface area decreased moderately to 242.187 m^2 g^{-1}, corresponding to a reduction of approximately 6.6%. In contrast, the total pore volume increased markedly from 0.1903 to 0.2999 cm^3g^{-1}, while the average pore diameter increased from 2.935 to 4.953 nm. Thus, the Cu/FCC catalyst retained approximately 93.4% of BET surface area while exhibiting a larger accessible pore volume and average pore diameter.

The moderate decrease in BET surface area after Cu impregnation is consistent with partial occupation or coverage of the FCC surface by deposited Cu-containing species. XRF analysis confirmed that the measured Cu content increased from 0.0074 wt% in the parent FCC to 0.689 wt% in the Cu/FCC catalyst. Rather, the simultaneous increase in total pore volume and average pore diameter indicates a redistribution of the N_2-accessible pore structure toward larger pores following impregnation. A similar trend was reported by (Charusiri et al., 2023) for Cu-modified spent FCC, where the surface area decreased slightly from 117.9 to 116.3 m^2 g^{-1}, the total pore volume increased from 0.12 to 0.13 cm^3 g^{-1} and the average pore size increased from 4.36 to 4.55 nm. Their XRF analysis also showed an actual Cu content of approximately 0.461 wt% despite a higher nominal Cu impregnation level. These similarities support the interpretation that relatively low measured

Table 4. Textural properties of FCC and Cu/FCC catalysts

Sample	S_{BET} (m^2/g)	Total pore volume (cm^3/g)	Average pore diameter (nm)
Fresh FCC	259.343	0.1903	2.935
Fresh Cu/FCC (5 wt%)	242.187	0.2999	4.953
Spent FCC	4.900	0.00675	5.512
Spent Cu/FCC	5.243	0.00994	7.588

Cu incorporation can modify the accessible pore environment without severely destroying the FCC framework. The BET surface area of spent FCC decreased from 259.343 to only 4.900 m^2 g^{-1}, representing a loss of approximately 98.1%, while the corresponding total pore volume decreased by approximately 96.5%, from 0.1903 to 0.00675 cm^3 g^{-1}. Similarly, the surface area of Cu/FCC decreased from 242.187 to 5.243 m^2 g^{-1} after reaction, corresponding to a reduction of approximately 97.8%, and its pore volume decreased from 0.2999 to 0.009945 cm^3 g^{-1}, or approximately 96.7%. These large reductions indicate a severe loss of N_2-accessible porosity during catalytic pyrolysis. The observed decrease in accessible surface area and pore volume is consistent with pore blockage by reaction-derived deposits and with possible changes in the catalyst structure during thermal exposure. (Almas et al., 2019). Their study showed that pore blockage and structural changes both contribute to FCC catalyst deactivation. Accordingly, the very large decrease in surface area observed for the present spent catalysts is consistent with extensive obstruction of the accessible pore system, although BET analysis alone cannot distinguish carbonaceous deposits from other causes of pore blockage or structural alteration. Interestingly, the average pore diameter increased after catalytic use, reaching 5.512 nm for spent FCC and 7.588 nm for spent Cu/FCC. Spent Cu/FCC retained a slightly larger surface area and pore volume than spent FCC. The surface area of spent Cu/FCC was 5.243 m^2 g^{-1} compared with 4.900 m^2 g^{-1} for spent FCC, while its pore volume was 0.009945 cm^3 g^{-1} compared with 0.00675 cm^3 g^{-1}. These differences correspond to approximately 7.0% higher accessible surface area and 47.3% higher accessible pore volume in spent Cu/FCC.

Physicochemical properties of pyrolysis liquid products

The physicochemical properties of the liquid products obtained from catalytic pyrolysis of waste lubricating oil are summarized in Table S3 of the Supplementary Information. The density of the produced liquid ranged from 0.82-0.86 g cm^{-3}, indicating substantial conversion of the original high-molecular-weight lubricating oil (Figure 3) into lighter hydrocarbon fractions. Similar studies have demonstrated that pyrolysis of waste engine and lubricating oils can generate liquid products with physicochemical properties approaching those of conventional petroleum-derived fuels. (Ahmad et al., 2016) evaluated density, viscosity, API gravity, calorific value, diesel index, and cetane-related properties of liquid products obtained from catalytic pyrolysis of spent lubricating oil and demonstrated that appropriately catalyzed pyrolysates can exhibit fuel properties comparable to diesel fuel.

The calorific value obtained in the present study ranged from 10,748 to 10,950 cal g^{-1}, corresponding to approximately 44.97–45.81 MJ kg^{-1}. This relatively high heating value indicates that the produced pyrolysis oil retained substantial chemical energy from the original lubricating-oil feedstock. (Santhoshkumar and Ramanathan, 2020) reported that waste-engine-oil-derived microwave pyrolysis oil exhibited calorific value and chemical characteristics comparable to diesel fuel, and subsequently demonstrated its applicability in a compression-ignition engine. (Maceiras et al., 2017) demonstrated that pyrolytic distillation can convert waste engine oil into diesel-like products whose physicochemical properties can approach those required for

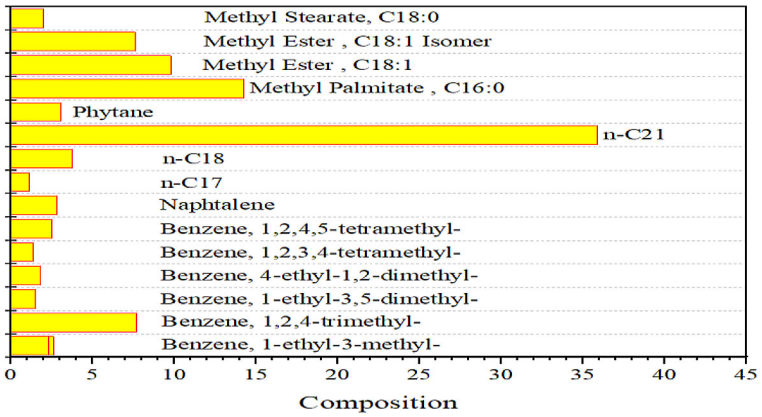

Figure 3. Composition of waste lubricant oil

practical engine fuels. Consequently, the calorific values measured in the present work support the potential use of the liquid product as an alternative diesel-like fuel or fuel precursor. Nevertheless, direct classification as commercial diesel requires additional verification of viscosity, flash point, cetane number, sulfur content, distillation curve, oxidation stability, and other relevant fuel-quality parameters.

The addition of FCC significantly increased the liquid yield from 72.56% under non-catalytic conditions to 85.21%, corresponding to an increase of 12.65 percentage points (Table 5). This result demonstrates the important contribution of the acidic catalytic sites of FCC to the conversion of high-molecular-weight hydrocarbons into lower-boiling condensable compounds. A similar catalytic effect has been demonstrated by (Afriansyah et al., 2022) employed zeolite catalysts for the pyrolysis of lubricant waste and reported that catalytic cracking facilitated the conversion of the waste hydrocarbon feed into liquid fuel at temperatures between 250 and 350 °C.Further modification of FCC with Cu increased the liquid yield from 85.21 to 91.04%, corresponding to an additional increase of 5.83 percentage points. Compared with thermal pyrolysis, Cu/FCC increased the total liquid yield by 18.48 percentage points, or approximately 25.5% on a relative basis. This result suggests that incorporation of Cu modifies the catalytic functionality of the FCC material and promotes conversion pathways favorable to the formation of condensable hydrocarbons. (Jin et al., 2023) demonstrated that incorporation of Cu into a zeolitic catalyst decreased the apparent activation energy of pyrolysis from 190.73 to 147.95 kJ mol^{-1} and reduced the initial pyrolysis temperature from approximately 410 to 360 °C. The Cu-containing zeolite also affected the distribution of liquid and gaseous hydrocarbons. Their mechanistic analysis indicated that the acidic sites promote β-cleavage through carbenium-ion pathways, followed by reactions including dehydrocyclization, oligomerization, and aromatization

Process optimization

The experimental liquid yields obtained from the catalytic pyrolysis of waste lubricating oil under different catalyst loadings and reaction times are summarized in Table 6. The reaction temperature was fixed at 350 °C throughout the CCD experiments to isolate the effects of catalyst loading and reaction time without introducing temperature as an additional independent variable. The selection of this temperature was supported by previous studies on waste lubricating oil conversion. Aburas et al. (2015) reported that relatively low-temperature operation is favorable when the objective is to maximize distillate products from waste lubricating oil pyrolysis. In addition, (Elsawy et al., 2020) demonstrated that increasing the reaction temperature during hydrocracking of feedstocks containing waste lubricating oil enhanced the formation of lighter gasoline and LPG fractions at the expense of kerosene- and diesel-range products. These findings support the use of 350 °C as a moderate fixed operating temperature that provides sufficient thermal energy for volatilization and catalytic transformation while limiting excessive secondary cracking toward lighter non-condensable products. Accordingly, 350 °C was treated as a controlled operating condition rather than an RSM-optimized variable. Fixing the temperature allowed the CCD to focus specifically on the individual, interaction, and quadratic effects of catalyst loading and reaction time on liquid-product recovery. Nevertheless, because liquid recovery at 350 °C may involve both volatilization-condensation of compounds initially present in the WLO and catalytic transformation of higher-molecular-weight species, the recovered liquid fraction was interpreted as condensable liquid yield rather than as a direct quantitative measure of chemical cracking conversion.

Based on the verified final dataset used for statistical analysis, the liquid yield ranged from 79.22 to 90.00%. The highest experimental liquid yield of 90.00% was obtained at a catalyst loading of 3.00% (w/v) and a reaction time of 60 min, whereas

Table 5. Effect of catalyst on liquid yield and heating value

Catalyst	Liquid yield (%)	Caloric Value (cal/g)
Thermal (Without Catalyst)	72.56	10.748,30
FCC	85.21	10.897,70
Cu/FCC	91.04	10.932,60

the lowest liquid yield of 79.22% was observed at 1.00% (w/v) catalyst loading and 60 min. The variation in liquid yield across the experimental conditions indicates that the response was governed by a nonlinear combination of catalyst loading and reaction time rather than by either factor independently.

At a catalyst loading of 3.00% (w/v), increasing the reaction time from 60 to 180 min decreased the liquid yield from 90.00 to 80.00%. This behavior suggests that prolonged thermal and catalytic exposure does not necessarily improve the recovery of condensable products. Extended residence time may promote further conversion of primary condensable vapors into lighter non-condensable species or other secondary products. However, because the experiments were performed at 350 °C, the recovered liquid fraction may reflect both volatilization and condensation of components originally present in the waste lubricating oil and catalytic transformation of higher-molecular-weight species. Therefore, the liquid yield is interpreted as the recovered condensable fraction and should not be regarded as a direct quantitative measure of chemical cracking conversion.

The verified dataset shows a nonlinear response to both factors. At 3.00% (w/v) catalyst loading, increasing reaction time from 60 to 180 min reduced liquid yield from 90.00 to 80.00%, consistent with increased secondary conversion or loss of condensable material at prolonged treatment. Because the experiment was conducted at 350 °C. Catalyst loading exhibits the strongest effect, indicating that increasing the amount of catalyst enhances cracking reactions due to the greater availability of active sites. These active sites facilitate the breakdown of long-chain hydrocarbons into lighter fractions, thereby increasing liquid yield.

The effects of catalyst loading and reaction time on liquid yield were evaluated using Response Surface Methodology based on a Central Composite Design. The three-dimensional response surface, observed-versus-predicted plot, and two-dimensional contour plot shown in Figure 4 illustrate the nonlinear relationship between the two operating variables and liquid yield. The response surface shows that increasing catalyst loading from the lower experimental level initially increases the predicted liquid yield, but further increases do not result in a continuous improvement. Reaction time exhibits a similar nonlinear response, with moderate reaction times favoring liquid recovery while prolonged treatment decreases the predicted response. This curvature is consistent with the statistically significant quadratic terms obtained from the regression analysis.

The response-surface analysis therefore demonstrates that maximum liquid recovery cannot be achieved simply by maximizing catalyst loading or extending reaction time. Rather, an appropriate combination of both variables is required. At relatively low catalyst loading, the available catalytic surface may be insufficient to strongly modify the vapor-phase product distribution. Conversely, excessive catalyst loading combined with prolonged reaction time may increase the extent of secondary transformations, thereby reducing the recovery of condensable liquid products. Additionally, the limited experimental range and inherent variability in measurements may contribute to the lack of statistical significance. The observed-versus-predicted relationship shown in Figure 4(b) was generated using the same final dataset used for regression and ANOVA (Table 7). The agreement between the measured and model-predicted values confirms

Table 6. Central composite design and experimental liquid yield

Run	Catalyst Loading (%w/v)	Time (min)	Liquid Yield (%)
1	1.00	60.00	79.22
2	1.00	180.00	83.02
3	3.00	60.00	90.00
4	3.00	180.00	80.00
5	0.59	120.00	81.48
6	3.41	120.00	86.00
7	2.00	35.15	82.46
8	2.00	204.85	81.73
9	2.00	120.00	88.50
10	2.00	120.00	88.00

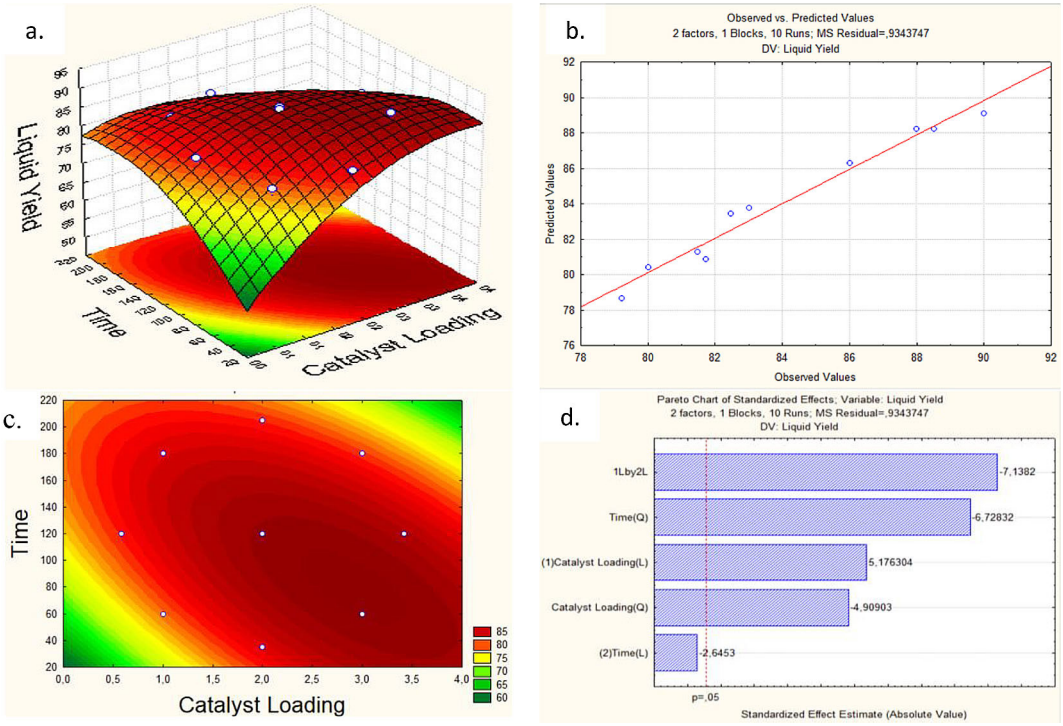

Figure 4. (a) Three-dimensional response surface plot for liquid yield; (b) observed versus predicted liquid yield;(c) two-dimensional contour plot showing the interaction between catalyst loading and reaction time; (d) Pareto chart of WLO pyrolysis

that the corrected quadratic model provides a suitable empirical representation of liquid-yield behavior within the experimental domain. The Pareto chart presented in Figure 5 further illustrates the relative contributions of the linear, interaction, and quadratic terms, with the interaction between catalyst loading and reaction time exerting the strongest statistical effect on the response. In contrast to liquid yield, the heating value of the recovered liquid products varied only within a relatively narrow range of approximately 44.97-45.81 MJ kg^{-1}. Because this variation was small compared with the changes in liquid recovery and the available experimental design did not provide sufficient independent information for a robust quadratic optimization of heating value, the heating-value results were interpreted descriptively rather than subjected to a separate RSM optimization model. A second-order quadratic regression model was selected because it can describe linear effects, interaction effects, and curvature behavior among process variables within the investigated design space. The corrected quadratic model predicted an optimum at 2.92% (w/v) catalyst loading and 79.81 min, corresponding to a predicted liquid yield of 89.37%. Experimental evaluation at the same operating condition produced a liquid yield of 92.10%. The quadratic regression model was statistically significant, with an F-value of 27.01 and a p-value of 0.0035. The coefficient of determination was R^2 = 0.9712, indicating that approximately 97.12% of the observed variation in liquid yield was described by the model. The adjusted R^2 of 0.9353 remained high after accounting for the number of model terms, supporting the adequacy of the quadratic representation within the investigated experimental domain. The residual sum of squares was 3.7375, while the model and total sums of squares were 126.1794 and 129.9169, respectively, satisfying the required relationship between model, residual, and total variability. The lack-of-fit test was not statistically significant (p = 0.2315), indicating that the unexplained model variation was not significantly greater than the experimental error estimated from the replicated center points.

The quadratic regression model was statistically significant (F = 27.01, p = 0.0035), with R^2 = 0.9712 and adjusted R^2 = 0.9353. Thus, approximately 97.1% of the observed variation in liquid yield was described by the quadratic model. Catalyst loading exhibited a significant linear effect (p = 0.0066), whereas the linear effect of reaction time was not statistically significant at the 95% confidence level (p = 0.0573). Nevertheless,

Table 7. ANOVA results for the quadratic regression model of WLO pyrolysis liquid yield

Source	Sum of squares	df	Mean square	F-value	p-value	
Model	126.18	5	25.24	27.01	0.0035	significant
X_1-Catalyst Loading	25.04	1	25.04	26.79	0.0066	
X_2-Reaction Time	6.54	1	6.54	7.00	0.0573	
AB	47.61	1	47.61	50.95	0.0020	
A^2	22.52	1	22.52	24.10	0.0080	
B^2	42.30	1	42.30	45.27	0.0025	
Residual	3.7375	4	0.9344			
Lack of Fit	3.61	3	1.20	9.63	0.2315	not significant
Pure Error	0.1250	1	0.1250			
Std. Dev.	0.9666					
Mean	84.04					
C.V. %	1.15					

reaction time contributed substantially through its significant quadratic term (B^2, p = 0.0025) and its significant interaction with catalyst loading (AB, p = 0.0020). The interaction term exhibited the largest F-value (50.95), demonstrating that the effect of catalyst loading depended strongly on reaction time. The adequacy of the quadratic regression model was further evaluated through residual analysis. The normal probability plot showed that the residual values followed an approximately linear distribution, indicating that the assumption of residual normality was satisfied. Furthermore, the residual versus predicted value plot showed a random distribution of residuals without obvious patterns, confirming the assumption of constant variance. These diagnostic evaluations indicate that the developed quadratic model was statistically appropriate for describing the relationship between catalyst loading, reaction time, and liquid yield.

The adequacy of the developed response surface model for predicting the liquid pyrolysis product was evaluated using diagnostic plots, including the predicted versus observed response plot and the normal probability plot of the regression effects. These diagnostic analyses were performed to verify the reliability of the regression model and to ensure that the fundamental assumptions of regression analysis were satisfied.

Figure 5(a) shows the normal probability plot used to evaluate the distribution of model effects and residual behavior. The data points follow an approximately linear trend along the expected normal distribution line, indicating that the residuals were normally distributed. The absence of significant deviation from linearity suggests that no major systematic errors or abnormal variations were present in the regression model. Therefore, the assumption of residual normality required for analysis of variance (ANOVA) was considered satisfied.

The normal distribution of residuals confirms that the developed quadratic model was statistically appropriate for evaluating the effects of catalyst loading and reaction time on yield. Together with the close agreement between predicted and experimental responses, these diagnostic results demonstrate that the RSM model provided an adequate prediction capability within the studied design space.

Figure 5(b) presents the relationship between the experimentally observed and RSM-predicted yield product. The data points are closely distributed along the diagonal reference line, indicating a strong agreement between the experimental measurements and the values predicted by the quadratic regression model. The limited deviation between observed and predicted values suggests that the developed model was capable of accurately describing the response behavior within the investigated experimental domain. This close correlation indicates that the variation in product yield caused by changes in catalyst loading and reaction time was adequately captured by the developed RSM model.

The high agreement between observed and predicted values also indicates that the regression equation provides an appropriate mathematical representation of the relationship between the independent variables and the yield product response.

Catalyst loading (factor A) had a statistically significant effect on liquid yield (p=0.0066),

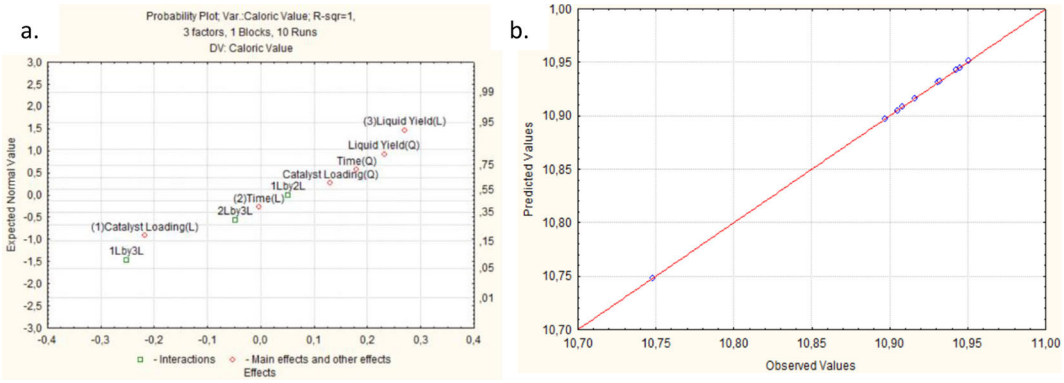

Figure 5. Statistical validation of the quadratic RSM model for predicting of pyrolysis liquid yield: (a) normal probability distribution of residuals and (b) residuals vs predicted

confirming that catalyst concentration is an important parameter influencing liquid recovery. In contrast, the linear effect of reaction time (factor B) was not statistically significant at the conventional 95% confidence level (p=0.0573). However, reaction time should not be considered unimportant, because its quadratic term (B^2) was highly significant (p=0.0025) and its interaction with catalyst loading (AB) was also significant (p=0.0020). The interaction term AB exhibited the highest F-value (50.95) among all model terms, indicating that the effect of catalyst loading on liquid yield strongly depends on reaction time, and vice versa. Therefore, optimization of either variable independently would not adequately describe the system. The significant quadratic terms A^2 and B^2 provide statistical confirmation of the curved response observed in the response-surface plots. In particular, the negative quadratic coefficients indicate that excessive catalyst loading or reaction time causes the response to decline after reaching an optimum region.

The experimentally measured liquid yield was 2.73 percentage points higher than the model-predicted response, corresponding to a relative deviation of approximately 3.05% (Table 8). The relatively small difference between the predicted and experimental responses indicates that the quadratic model satisfactorily identified the high-liquid-yield operating region. The experimental value exceeding the fitted model prediction does not invalidate the regression model because the quadratic equation represents a response surface fitted to all CCD observations, whereas an individual experimental measurement may deviate from the fitted response because of experimental variability. The experimental verification further demonstrates that a catalyst loading of approximately 2.92% (w/v) combined with a reaction time of approximately 79.81 min provides favorable conditions for condensable liquid recovery. The optimization results therefore confirm that maximum liquid recovery cannot be achieved simply by increasing catalyst loading or extending reaction time independently. Instead, an appropriate combination of the two variables is required to balance catalyst availability and reaction duration while limiting excessive secondary transformations.

The presence of statistically significant interaction and quadratic effects strongly supports this interpretation.The second-order polynomial regression equations for WLO catalytic pyrolysis, expressed in terms of coded variables, are presented in Equations 1:

$$Y_{Yield} = 88.250 + 1.769\mathrm{A} - 0.904\mathrm{B} - 3.450\ \mathrm{AB} - 2.219\ \mathrm{A}^2 - 3.042\ \mathrm{B}^2 \quad (8)$$

where: Y is the predicted liquid yield, A is the coded catalyst loading, and B is the coded reaction time.

The negative coefficients of the quadratic terms indicate a concave response surface and confirm the presence of an interior optimum rather than a continuously increasing response. Similarly, the negative interaction coefficient indicates that simultaneously increasing catalyst loading and reaction time beyond their favorable ranges can reduce liquid recovery.

Stationary-point analysis of the corrected quadratic model predicted an optimum at approximately 2.92% (w/v) catalyst loading and 79.81 min reaction time, corresponding to a maximum predicted liquid yield of approximately 89.37%. This optimum lies within the investigated design

Table 8. Comparison of RSM-predicted and experimentally measured liquid yield at the optimum condition

Parameter	Predicted optimum	Experimental result
Catalyst loading	2.92% (w/v)	2.92% (w/v)
Reaction time	79.81 Minutes	79.81 Minutes
Liquid yield	89.37 %	92.10 %

space. The predicted optimum is slightly lower than the highest individual experimental yield of 90.00%, which is reasonable because the quadratic regression model represents a fitted response surface across all experimental runs, whereas individual observations may deviate slightly from the fitted surface because of experimental residual variation. The response-surface analysis therefore demonstrates that maximum liquid recovery cannot be achieved simply by maximizing catalyst loading or extending reaction time. Rather, an appropriate combination of both variables is required. At relatively low catalyst loading, the available catalytic surface may be insufficient to strongly modify the vapor-phase product distribution. Conversely, excessive catalyst loading combined with prolonged reaction time may increase the extent of secondary transformations, thereby reducing the recovery of condensable liquid products.

Optimized conditions and comparative analysis

The optimized catalytic pyrolysis process produced a liquid fuel yield of 92.1% at a Cu/FCC catalyst loading of 2,92 wt% and a reaction time of 79 min. This result indicates that the combination of Cu-modified FCC catalyst and the selected reaction duration provided favorable conditions for converting waste lubricating oil into condensable hydrocarbon products. The high liquid yield obtained in this study compares favorably with several previously reported WLO pyrolysis systems, although differences in feedstock composition, reactor configuration, catalyst properties, reaction temperature, and definition of liquid yield should be considered when interpreting these comparisons. Reviews of WLO pyrolysis (Table 9) have similarly emphasized that catalyst characteristics and operating conditions strongly affect both pyro-oil yield and product quality (Singh et al., 2025).

The optimized catalytic pyrolysis process developed in the present study produced a liquid yield of 92.1% using 2.92 wt% Cu/FCC and a reaction time of 79 min. This result compares favorably with several previous investigations on the thermochemical conversion of waste lubricating and engine oils.research conducted by (Arpa et al., 2010) reported approximately 60% diesel-like fuel recovery from waste engine oil using pyrolitic distillation with Na_2CO_3, zeolite, and CaO additives. Although their process successfully produced a fuel with properties approaching those of diesel, the total recoverable diesel-like fraction was substantially lower than the liquid yield obtained in the present study.

Microwave-assisted pyrolysis has also demonstrated relatively high liquid recovery. Lam et al. obtained approximately 88 wt% pyrolysis oil from waste automotive engine oil, with the product exhibiting fuel-related properties comparable to conventional petroleum-derived transportation fuels. The liquid yield obtained in the present Cu/FCC catalytic system is therefore approximately percentage points higher than that reported for microwave pyrolysis, although the differences in heating mechanism and reactor configuration prevent a direct one-to-one comparison. (Sinağ et al., 2010) showed that pyrolysis temperature and catalyst type strongly influence product distribution. Their waste machinery oil experiments demonstrated that increasing temperature from 400 to 800 °C progressively increased gas formation while reducing pyrolytic-oil production. Catalytic runs using Ni/SiO_2 and HZSM-5 also produced lower liquid yields because catalytic cracking favored further conversion of condensable hydrocarbons into lighter gaseous species. This behavior supports the interpretation that the 2.92wt% Cu/FCC loading used in the present study may represent a favorable balance between primary cracking of heavy hydrocarbons and suppression of excessive secondary cracking.

Catalytic cracking substantially altered the physicochemical characteristics of the waste lubricating oil (Table 10). The most pronounced change was observed in kinematic viscosity,

Table 9. Comparison of WLO in Pyrolysis to Fuel at different studies

Study	Method	Catalyst	Liquid yield (%)	Conditions
This Study	Cataytic pyrolysis	Cu/FCC	92.1%	Catalyst loading :2.92 (w/v) Time: 79 Minutes
(Lesmana and Wu, 2015)	Catalytic pyrolysis	Spent zeolite catalyst	60%	Temperature: 370 °C
(Arpa et al., 2010)	Pyrolitic distillation	Na_2CO_3, zeolite, CaO	60%	Additive loading: 2–10 wt%; CaO 2 wt%
(Sinağ et al., 2010)	Catalytic pyrolysis	Ni/SiO_2; HZSM-5	72%at 400 °C (thermal); 60% catalytic	Tubular reactor; 400–800 °C; catalyst loading 5 wt%
(Lam et al., 2012)	Microwave-assisted pyrolysis	None	88%	Continuous microwave heating; 5 kW magnetron;
(El-Mekkawi et al., 2020)	Catalytic pyrolysis	Al_2O_3	90.7%	Catalyst: 2 wt%; temperature: 550 °C; oxygen-free autoclave
(Parapat et al., 2024)	Catalytic pyrolysis	Fe-Ni/TiO_2	54.1%	Temperature: 400 °C; 0.5 g catalyst/30 g WLO; N_2 atmosphere, 1 atm

which decreased from 53.94 to 4.97 cSt at 40 °C, corresponding to a reduction of approximately 90.8%. This substantial decrease provides strong evidence of the conversion of high-molecular-weight lubricant components into lower-molecular-weight hydrocarbons. The flash point decreased from 100 °C to 35 °C, further indicating an increased proportion of volatile hydrocarbon fractions after cracking. However, the decrease in flash point also implies increased flammability and associated handling and storage considerations.In contrast, the pour point increased from -30 °C to -9 °C, indicating less favorable low-temperature flow behavior of the cracking product. The product density at 15 °C was 0.83259 g cm^{-3}; however, the absence of feed-density data prevents calculation of the corresponding density change. In addition, the 90% recovery temperature exceeded 400 °C, preventing reliable determination of the calculated cetane index and indicating that a relatively heavy boiling fraction remained in the product. Overall, the cracking process considerably improved fluidity and increased volatility, although further separation or upgrading may be required to optimize cold-flow and distillation characteristics. The total nitrogen concentration decreased from 1258.193 to 375.484, corresponding to a reduction of approximately 70.16%. Similarly, total sulfur decreased from 2762.718 to 956.595, representing a reduction of approximately 65.37%. These results indicate that the cracking process promoted the removal or redistribution of heteroatom-containing compounds from the liquid phase. Nitrogen and sulfur containing species may have undergone thermal or catalytic decomposition and subsequently been transferred to gaseous products, coke/residue, or retained on the catalyst surface. The reduction in these heteroatoms is beneficial for improving the quality of the cracked liquid; however, the remaining sulfur content indicates that additional desulfurization or hydrotreating may still be required for applications requiring low-sulfur transportation fuels.

The comparison further shows that the 92.1% liquid yield obtained in the present study is among the higher values reported for WLO conversion, being slightly higher than the 90.7% obtained by (El-Mekkawi et al., 2020) using Al_2O_3 and substantially higher than the values reported by (Arpa et al., 2010; Lesmana and Wu, 2015; Parapat et al., 2024; Sinağ et al., 2010).

As shown in Figure 6 the GC-MS profile of the liquid product obtained under the optimum catalytic pyrolysis conditions. The chromatogram exhibits numerous peaks predominantly distributed within a retention-time range of approximately 20–32 min, indicating the presence of a complex mixture of medium- to high-boiling hydrocarbon compounds. The identified components include long-chain paraffinic hydrocarbons and alkyl-substituted aromatic compounds, reflecting extensive thermal and catalytic transformation of the original waste lubricating oil feedstock. The occurrence of compounds within the middle-distillate carbon-number range indicates that the resulting pyrolysis oil is enriched in hydrocarbons relevant to diesel-range applications. However, the product should be described as a hydrocarbon-rich pyrolysis oil rather than commercial diesel fuel, because additional fuel-quality parameters are required for definitive fuel classification.

Table 10. Comparison of physicochemical properties of waste lubricating oil feed and optimum catalytic cracking product

Property	Method	Unit	Waste oil	Optimum product
Pour Point	ASTM D97	°C	-30	-9
Flash Point	ASTM D93	°C	100	-65
Kinematic Viscosity at 40 ℃	ASTM D455	$mm^2\ s^{-1}$ (cSt)	53.94	4.97
Density at 15 ℃	ASTM D4052	$g\ cm^{-3}$	-	0.83259
Nitrogen	-	-	1258.193	375.484
Sulfur	-	-	2762.718	956.595

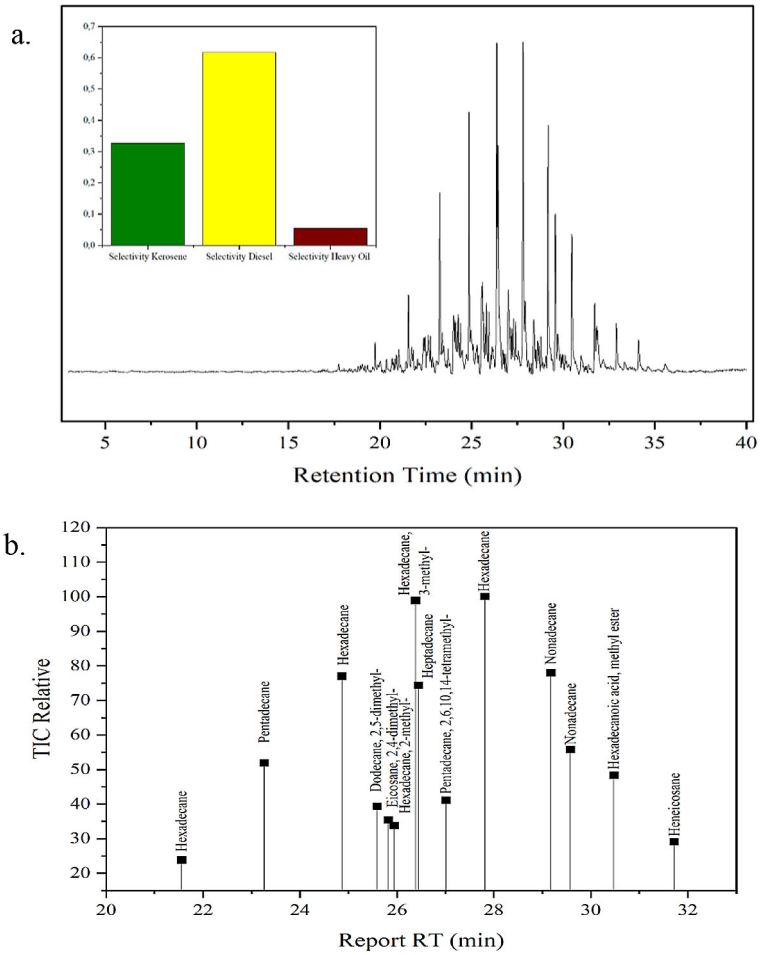

Figure 6. (a) Product distribution WLO pyrolysis, (b) peak of GCMS in optimum condition

Thermal gravimetric analysis

Thermogravimetric analysis revealed a pronounced difference between the fresh/impregnated catalysts and their corresponding spent forms. Fresh FCC exhibited a total mass decomposition of 18.88%, whereas spent FCC showed a considerably higher mass loss of 29.36%. Similarly, the total decomposition increased from 14.69% for the impregnated Cu/FCC catalyst to 29.07% after its use in waste lubricating oil cracking. These increases indicate substantial accumulation of thermally decomposable species during catalytic conversion, potentially including strongly adsorbed hydrocarbons and carbonaceous deposits (Figure 7).

This observation is consistent with the catalytic behavior reported by Charusiri et al. (2023), who demonstrated that Cu modification of spent FCC increased catalyst acidity and promoted C-C bond cleavage and secondary cracking during spent lubricating oil conversion. Their study also indicated that excessive catalytic activity

may favor gas and carbonaceous-coke formation and that catalytic performance deteriorates after repeated reuse. A similar trend was observed for the Cu-modified catalyst. The impregnated Cu/FCC catalyst exhibited the lowest total mass loss (14.69%) and the highest residual fraction (85.31%), whereas the spent Cu/FCC catalyst showed a considerably higher total mass loss of 29.07% and a residual fraction of 70.93%. The increase of approximately 14.38 percentage points after the reaction indicates substantial accumulation of thermally decomposable species on the catalyst surface during catalytic cracking. The corresponding thermogravimetric data are summarized in Table S3 of the Supplementary Information.

Interestingly, the overall mass losses of spent FCC (29.36%) and spent Cu/FCC (29.07%) were very similar, indicating that Cu modification did not substantially alter the total amount of thermally removable material accumulated after reaction. However, the decomposition profiles were different. Spent Cu/FCC exhibited two distinct mass-loss stages (24.08 and 5.00%), with DTG features centered at approximately 255 and 432 °C, whereas spent FCC was dominated by a major decomposition region near 278 °C. This suggests that Cu modification may influence the nature and thermal stability distribution of deposited species rather than simply suppressing their total formation. Such behavior can be associated with modification of the catalyst acid-site environment by Cu. Previous studies of Cu-modified zeolites have shown that moderate Cu incorporation can increase the concentration of acidic sites while largely preserving the crystalline framework, thereby modifying hydrocarbon cracking pathways and product distributions. Accordingly, the additional higher-temperature DTG feature observed for the spent Cu/FCC catalyst may reflect the formation of a more thermally stable fraction of surface deposits. Nevertheless, definitive attribution of this region to coke requires consideration of the TGA atmosphere and complementary carbon characterization. The corresponding TGA/DTG profiles are presented in Figure S3 of the Supplementary Information.

Although spent FCC and spent Cu/FCC exhibited similar overall mass losses (29.36 and 29.07%, respectively), their decomposition behavior differed. Spent Cu/FCC showed two distinguishable mass-loss stages, accounting for 24.08 and 5.00%, whereas spent FCC was characterized predominantly by a single decomposition stage. This behavior suggests that Cu modification may influence the nature or thermal stability distribution of surface deposits rather than substantially changing their overall quantity. The final residual fraction followed the order impregnated Cu/FCC (85.31%) > fresh FCC (81.12%) > spent Cu/FCC (70.93%) > spent FCC (70.64%). However, assignment of individual mass-loss regions specifically to moisture, adsorbed hydrocarbons, or coke requires consideration of the corresponding temperature ranges, DTG profiles, and TGA atmosphere.

Process simulation

The catalytic pyrolysis process was simulated using Aspen HYSYS to evaluate material distribution, phase behavior, product separation, and overall process performance (Figure 8). The thermodynamic property package used in the simulation was Peng-Robinson, selected for the hydrocarbon-rich composition of the simulated streams. The chemical components used in the HYSYS simulation were selected directly from the compounds identified experimentally by gas chromatography-mass spectrometry (GC-MS). The GC-MS analysis identified a mixture of aromatic hydrocarbons, aliphatic hydrocarbons, and oxygenated compounds. The relative composition of the components was derived from

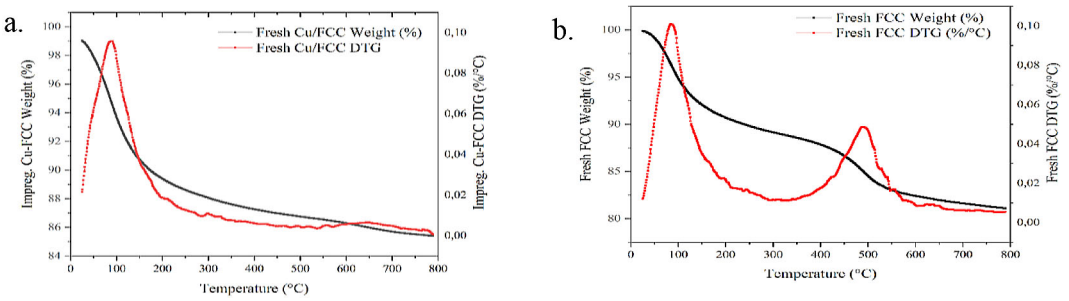

Figure 7. TGA profiles of; (a) fresh Cu/FCC, (b) FCC catalysts

the normalized GC-MS peak-area percentages and used as the basis for defining the simulated product stream was tabulated in Table S4 of the supplementary files.

Therefore, the hydrocarbon mixture in the HYSYS model was represented using experimentally identified pure components rather than hypothetical components. This approach enabled the simulated stream composition to reflect the experimentally observed hydrocarbon distribution of the pyrolysis liquid product. The oil pyrolysis process was simulated using Aspen HYSYS to evaluate the thermal conversion of the hydrocarbon feed into condensable pyrolysis oil and non-condensable pyrolysis gas. The simulation flowsheet consisted of a feed heater (E-100), a pyrolysis reactor (CRV-100), three sequential cooling and vapor-liquid separation stages (E-101/V-100, E-102/V-101, and E-103/V-102), and a mixer (MIX-100) for combining the recovered liquid fractions. The feed was initially introduced at 25 °C and 101.3 kPa with a mass flow rate of 1.263 kg/h. Prior to the pyrolysis reaction, the feed was heated to 350 °C in E-100 to provide sufficient thermal energy for the decomposition of the heavier hydrocarbon molecules. The heated feed entered the pyrolysis reactor at 350 °C and atmospheric pressure. The mass flow rate remained approximately constant through the reactor, whereas the molar flow rate increased from 5.179 kmol/h at the reactor inlet to 9.093 kmol/h at the outlet. This increase of approximately 75.6% indicates molecular fragmentation, where relatively large hydrocarbon molecules were converted into a greater number of lower-molecular-weight molecules. The reactor outlet temperature decreased to approximately 284.9 °C, after which the product stream was subjected to staged cooling and condensation for pyrolysis oil recovery. The hot vapor stream was cooled in E-101 from approximately 284.9 to 65 °C. The reduction in temperature caused a substantial fraction of the condensable hydrocarbons to enter the liquid phase. Separation in V-100 produced approximately 1.138 kg/h of Oil-1, corresponding to approximately 90.10 wt% of the original feed. Only 124.3 kg/h remained in the vapor phase and was transferred to the subsequent cooling stage. The gas stream leaving V-100 was further cooled from 65 to 25 °C in E-102. This secondary cooling stage condensed an additional 2.019 kg/h of pyrolysis oil. Following separation in V-101, approximately 122.2 kg/h remained as non-condensable pyrolysis gas. The liquid streams from V-100 and V-101 were subsequently combined in MIX-100, resulting in a total pyrolysis oil production of approximately 1.140 kg/h. The corresponding process stream data are summarized in Table S5 of the Supplementary Information. The gas formed at V-100 was cooled further from 65 to 25 °C in E-102. This secondary cooling stage condensed only an additional 2.019 kg/h of pyrolysis oil. After separation in V-101, approximately 122.2 kg/h remained as non-condensable pyrolysis gas. The liquid streams from V-100 and V-101 were subsequently combined in MIX-100, resulting in a total pyrolysis oil production of approximately 1.140 kg/h (Table 11).

The resulting mass closure was approximately 99.94%, indicating good consistency of the overall material balance. The small difference from 100% is mainly attributable to rounding of the stream values reported by the simulator. Approximately 99.82% of the total pyrolysis oil was obtained as Oil-1 from V-100. The simulated feed consisted predominantly of relatively high-carbon-number hydrocarbons. The main components included n-C21, n-C19, n-C16, toluene, n-C18, n-C20, and n-C17. Following pyrolysis,

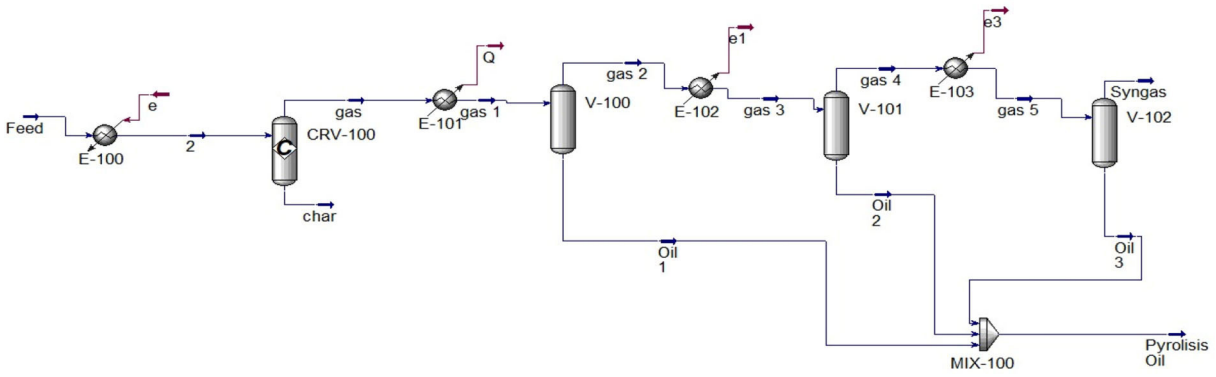

Figure 8. Simulation of Pyrolysis by HYSYS

significant changes in hydrocarbon distribution were observed. The fractions of n-C21 and n-C19 decreased considerably, whereas the concentrations of n-C16 and n-C17 increased tabulated in Table S6 of the supplementary files. The decrease in heavier hydrocarbons was particularly evident for n-C21, which decreased from 33.35 mol% in the feed to 10.21 mol% in the pyrolysis oil, and for n-C19, which decreased from 23.77 to 9.71 mol%. Conversely, n-C16 increased substantially from 17.34 to 41.53 mol%, becoming the dominant component of the final liquid product. The increase in n-C17 from 1.30 to 17.40 mol% further indicates conversion toward intermediate-carbon-number hydrocarbon fractions. The combined C16-C21 fraction accounted for approximately 87.1 mol% of the final pyrolysis oil. Therefore, the liquid product obtained from the simulation was predominantly composed of middle-to-heavy hydrocarbon fractions. This carbon-number distribution overlaps substantially with the middle-distillate range. However, the simulated product is more appropriately described as pyrolysis oil containing diesel-range hydrocarbons, rather than directly classified as commercial diesel fuel. Additional fuel-property characterization would be required for such a classification. Aspen HYSYS simulation predicted effective thermal conversion of the oil feed into a predominantly liquid pyrolysis product. At a feed rate of 1.263 kg/h and a pyrolysis temperature of 350 °C, the process produced approximately 1.140 kg/h of pyrolysis oil and 122.2 kg/h of non-condensable pyrolysis gas, corresponding to yields of 90.26 and 9.68 wt%, respectively. The increase in molar flow across the reactor, reduction of heavier C19-C21 components, formation of lighter gaseous hydrocarbons, and accumulation of C16-C17 components in the liquid product collectively indicate thermal decomposition of the original hydrocarbon feed.

The simulated thermal duties and specific energy requirements of the Aspen HYSYS process units are summarized in Table 12. The feed heater (E-100) exhibited the highest positive heat duty, requiring 848.7 kJ h^{-1}, equivalent to approximately 0.236 kW. Based on the simulated pyrolysis-oil production rate of 0.7028 kg h^{-1}, this corresponds to a specific heating demand of approximately 1.208 MJ kg^{-1} of liquid product. This heating requirement is primarily associated with raising the feed temperature from 25 °C to the fixed process temperature of 350 °C before entering the conversion reactor. Among the cooling units, E-101 accounted for the dominant heat-removal requirement, with a duty of 608.6 kJ h^{-1} or approximately 0.169 kW. This unit cools the hot reactor effluent before the first vapor-liquid separation step and therefore carries most of the condensation-related thermal load. In contrast, E-102 required only 5.469 kJ h^{-1}, while E-103 exhibited essentially zero additional duty under the converged simulation conditions. The total simulated cooling duty was approximately 614.1 kJ h^{-1}, corresponding to 0.874 MJ kg^{-1} of recovered liquid product was tabulated in Table S7 of the supplementary files. The difference between heating and cooling duties reflects the thermal structure of the modeled process. However, such heat recovery was not explicitly implemented in the present HYSYS model and therefore should be considered a process-development opportunity rather than a demonstrated energy-saving result.

The calculated specific heating demand of 1.208 MJ kg^{-1} liquid should be interpreted as an idealized process duty obtained from the HYSYS simulation rather than as the total energy consumption of the experimental or commercial process. Accordingly, the value provides a useful process-level basis for comparing thermal requirements among unit operations, but it should not be used directly as the overall plant energy consumption.

This distinction is particularly important for assessing the feasibility of waste-lubricating-oil conversion. (Moses et al., 2023) emphasized the need for techno-economic and life-cycle assessment when evaluating WLO catalytic-treatment technologies, indicating that process performance should be considered together with energy and utility requirements. Similarly, (Aburas et al., 2015) reported that relatively low-temperature operation can be favorable when the objective is to maximize distillate products from waste lubricating oil pyrolysis. In the present process, the use of a fixed temperature of 350 °C therefore represents a moderate thermal condition, while the HYSYS duty analysis provides an initial quantitative estimate of the heating and cooling requirements associated with that operating condition.

Preliminary techno-economic considerations

The practical implementation of catalytic pyrolysis of waste lubricating oil depends not only on liquid-product yield but also on feedstock availability, catalyst cost, energy consumption,

Table 11. Flow product simulation

Product	Mass flow (kg/h)	Yield (wt%)
Oil-1	1,138	90.10
Oil-2	2.019	0.16
Oil-3	Negligible	0
Total pyrolysis oil	1.140	90.26
Pyrolysis gas	122.2	9.68
Char/coke	Not modeled	-

Table 12. Summary of optimum process in HYSYS simulation

Parameter	Simulation result
Feed flow rate	1.263 kg/h
Feed temperature	25 °C
Pyrolysis reactor inlet temperature	350 °C
Reactor pressure	101.3 kPa
Reactor inlet molar flow	5.179 kmol/h
Reactor outlet molar flow	9.093 kmol/h
Increase in molar flow	75.6%
Pyrolysis oil production	1,140 kg/h
Pyrolysis oil yield	90.26 wt%
Pyrolysis gas production	122.2 kg/h
Pyrolysis gas yield	9.68 wt%
C16-C21 in pyrolysis oil	87.1 mol%
Liquid recovered in first separator	99.82% of total liquid

product upgrading requirements, and opportunities for process integration. Therefore, although a complete techno-economic analysis was beyond the scope of the present laboratory-scale study, several preliminary economic considerations can be identified.

Waste lubricating oil represents a potentially valuable feedstock because its conversion simultaneously addresses waste-management requirements and recovers hydrocarbon-containing material. However, feedstock collection, transportation, storage, filtration, dehydration, and other pretreatment steps may contribute to operating costs. The economic benefit associated with WLO utilization will therefore depend strongly on local collection infrastructure and the consistency of feedstock quality.

Catalyst-related costs represent another important consideration. The present process employs fresh FCC modified with Cu, requiring both FCC material and a copper precursor as well as preparation steps such as impregnation and thermal treatment. Although Cu modification improved catalytic performance, the economic benefit of this improvement must ultimately be balanced against catalyst preparation costs, catalyst lifetime, deactivation rate, and regeneration requirements. Repeated catalyst reuse and regeneration studies are therefore necessary before catalyst-related operating costs can be reliably estimated.

Thermal-energy demand is also expected to be an important operating-cost component. In the present laboratory system, the reactor was externally heated using LPG and operated at 350 °C, with reaction times ranging from 60 to 180 min. Such batch operation may involve significant heat losses and relatively high specific energy consumption compared with a larger, continuously operated and thermally integrated system. At larger scale, improved reactor insulation, heat recovery from hot product streams, utilization of non-condensable gases as an auxiliary energy source, and continuous processing could potentially reduce external fuel requirements. These possibilities, however, require experimental verification and were not quantified in the present study.

Downstream upgrading is another important economic factor. Although the liquid product exhibits high calorific value and contains a substantial diesel-range hydrocarbon fraction, its measured properties alone are insufficient to establish direct compliance with commercial diesel standards. Additional processing, such as fractionation, stabilization, removal of undesirable compounds, or hydrotreating, may therefore be required depending on the intended application. Such upgrading would increase both capital and operating expenditures and, in the case of hydrotreating, would introduce additional hydrogen and energy requirements.

From a process-benefit perspective, the relatively high liquid recovery obtained in this study indicates that a substantial fraction of the waste feed can be converted into a potentially valuable hydrocarbon-rich product. However, economic

viability cannot be inferred directly from liquid yield alone. The overall process economics will depend on the market value of the recovered liquid, waste-oil acquisition or disposal-credit conditions, catalyst lifetime, fuel and utility consumption, product-upgrading requirements, treatment of residue and non-condensable gases, and plant scale.

Consequently, the present results should be interpreted as demonstrating the technical feasibility and process potential of Cu/FCC-assisted WLO pyrolysis rather than establishing commercial economic viability. Future studies should perform a detailed techno-economic analysis incorporating capital expenditure (CAPEX), operating expenditure (OPEX), energy consumption, catalyst replacement and regeneration, product upgrading, waste-management credits, and product revenue. Economic indicators such as minimum fuel selling price, net present value, internal rate of return, and payback period should subsequently be evaluated using data obtained from pilot- or continuous-scale operation.

CONCLUSIONS

This study demonstrates that Cu-modified FCC can enhance the catalytic conversion of waste lubricating oil into a hydrocarbon-rich liquid product dominated by diesel-range components. The combined use of catalyst modification, response surface optimization, and process simulation provides a systematic framework for evaluating both catalytic performance and process behavior. The results indicate that catalyst loading and reaction time interact strongly and should therefore be optimized simultaneously rather than independently. The observed curvature in the response surface also suggests that increasing catalyst dosage or extending reaction time beyond the favorable operating region does not necessarily improve liquid recovery and may instead promote secondary cracking and gas formation. From an engineering perspective, the integration of experimental product composition with Aspen HYSYS provides a useful basis for examining downstream separation, condensation, material distribution, and overall process consistency. However, the simulation should be interpreted as a process-level representation based on experimentally derived inputs rather than an independent kinetic prediction of pyrolysis chemistry.

The produced liquid exhibited a high energy content and a hydrocarbon distribution relevant to diesel-range fuel applications. Nevertheless, additional upgrading and comprehensive fuel-quality testing are required before the product can be considered equivalent to, or compliant with, diesel specifications. Overall, the results support the technical potential of Cu/FCC-assisted pyrolysis as a waste-lubricating-oil valorization pathway. Further development should focus on catalyst durability, continuous processing, energy efficiency, product upgrading, and pilot-scale validation to determine whether the process can be translated from laboratory operation to practical industrial application.

Acknowledgments

This research was funded by the Indonesian Endowment Fund for Education (LPDP), on behalf of the Indonesian Ministry of Higher Education, Science and Technology, and managed under the EQUITY Program (Contract No. 4306/B3/DT.03.08/2025). The authors also gratefully acknowledge Technology and Innovation Pertamina and the Catalysis Science and Technology Research Centre (PutraCat), Universiti Putra Malaysia, for their technical support, research facilities, and scientific contributions to this work.

REFERENCES

1. Aburas, H., Bafail, A., Demirbas, A. (2015). The pyrolizing of waste lubricating oil (WLO) into diesel fuel over a supported calcium oxide additive. *Petroleum Science and Technology*, *33*(2), 226–236. https://doi.org/10.1080/10916466.2014.973604
2. Afriansyah, H., Ramlan, M. R., Roulina T, M., Bow, Y., Fatria. (2022). Pyrolysis of lubricant waste into liquid fuel using zeolite catalyst. *International Journal of Research in Vocational Studies (IJRVOCAS)*, *1*(4), 26–31. https://doi.org/10.53893/ijrvocas.v1i4.72
3. Ahmad, I., Khan, R., Ishaq, M., Khan, H., Ismail, M., Gul, K., Ahmad, W. (2016). Catalytic pyrolysis of used engine oil over coal ash into fuel-like products. *Energy and Fuels*, *30*(1), 204–218. https://doi.org/10.1021/acs.energyfuels.5b02316
4. Al-jabiri, A. A., Balla, H. H., Al-zuhairy, M. S., Alahmer, H., Al-Manea, A., Al-Rbaihat, R., Alahmer, A. (2024). Applied AMT machine learning and multi-objective optimization for enhanced performance and reduced environmental impact of sunflower oil biodiesel in compression ignition engine.

International Journal of Thermofluids, *24*(September 2024), 100838. https://doi.org/10.1016/j.ijft.2024.100838

5. Al-Rbaihat, R. (2025). Sensitivity analysis of a Hybrid PV-WT hydrogen production system via an electrolyzer and fuel cell using TRNSYS in coastal regions: A case study in Perth, Australia. *Energies*, *18*(12). https://doi.org/10.3390/en18123108
6. Almas, Q., Naeem, M. A., Baldanza, M. A. S., Solomon, J., Kenvin, J. C., Müller, C. R., Teixeira Da Silva, V., Jones, C. W., Sievers, C. (2019). Transformations of FCC catalysts and carbonaceous deposits during repeated reaction-regeneration cycles. *Catalysis Science and Technology*, *9*(24), 6977–6992. https://doi.org/10.1039/c9cy01680e
7. Arpa, O., Yumrutas, R., Demirbas, A. (2010). Production of diesel-like fuel from waste engine oil by pyrolitic distillation. *Applied Energy*, *87*(1), 122–127. https://doi.org/10.1016/j.apenergy.2009.05.042
8. Boro, B., Tiwari, P. (2025). Pyrolysis of waste printed circuit board fragments: Response surface methodology optimization and effect of temperature on product characteristics. *Energy*, *319*(August 2024), 134892. https://doi.org/10.1016/j.energy.2025.134892
9. Botas, J. A., Moreno, J., Espada, J. J., Serrano, D. P., Dufour, J. (2017). Recycling of used lubricating oil: Evaluation of environmental and energy performance by LCA. *Resources, Conservation and Recycling*, *125*(January), 315–323. https://doi.org/10.1016/j.resconrec.2017.07.010
10. Charusiri, W., Phowan, N., Permpoonwiwat, A., Vitidsant, T. (2023). Catalytic copyrolysis of used waste plastic and lubricating oil using Cu-modification of a spent fluid catalytic cracking catalyst for diesel-like fuel production. *ACS Omega*, *8*(43), 40785–40800. https://doi.org/10.1021/acsomega.3c05823
11. Ćurković, L., Cerjan-Stefanović, Š., Filipan, T. (1997). Metal ion exchange by natural and modified zeolites. *Water Research*, *31*(6), 1379–1382. https://doi.org/10.1016/S0043-1354(96)00411-3
12. Dewi, S. P., Alsakinah, R., Sara, S. A., Amrina, D. H. (2022). Pajak lingkungan sebagai upaya pengendalian pencemaran udara dari gas buang kendaraan bermotor Di Indonesia. *Jurnal Ilmiah Ekonomi Dan Pajak (EJAK)*, *2*(1), 7–13. https://ojs-ejak.id/index.php/
13. El-Mekkawi, S. A., El-Ibiari, N. N., Attia, N. K., El-Diwani, G. I., El-Ardy, O. A., Morsi, A. K. E. (2020). Reducing the environmental impact of used lubricating oil through the production of fuels by pyrolysis. *Environmental Nanotechnology, Monitoring and Management*, *14*(May), 100308. https://doi.org/10.1016/j.enmm.2020.100308
14. El-sawy, M. S., Hana, S. A., Ashour, F., Aboulfotouh, T. M. (2020). *Co-hydroprocessing and hydrocracking of alternative feed mixture (vacuum gas oil / waste lubricating oil / waste cooking oil) with the aim of producing high quality fuels*. *269*(June 2019). https://doi.org/10.1016/j.fuel.2020.117437
15. European Commission. (2021). *Report From The Commission To The European Parliament And The Council*. 167–186. https://doi.org/10.2779/948514
16. Jin, J., Sun, J., Lv, K., Hou, Q., Guo, X., Liu, K., Deng, Y., Song, L. (2023). Catalytic pyrolysis of oil shale using tailored Cu@zeolite catalyst and molecular dynamic simulation. *Energy*, *278*(PA), 127858. https://doi.org/10.1016/j.energy.2023.127858
17. Lam, S. S., Russell, A. D., Lee, C. L., Chase, H. A. (2012). Microwave-heated pyrolysis of waste automotive engine oil: Influence of operation parameters on the yield, composition, and fuel properties of pyrolysis oil. *Fuel*, *92*(1), 327–339. https://doi.org/10.1016/j.fuel.2011.07.027
18. Lesmana, D., Wu, H. S. (2015). Pyrolysis of waste oil in the presence of a spent catalyst. *Journal of Environmental Chemical Engineering*, *3*(4), 2522–2527. https://doi.org/10.1016/j.jece.2015.09.019
19. Liu, X., Khinast, J. G., Glasser, B. J. (2008). A parametric investigation of impregnation and drying of supported catalysts. *Chemical Engineering Science*, *63*(18), 4517–4530. https://doi.org/10.1016/j.ces.2008.06.013
20. Lu, G., Lu, X., Liu, P. (2020). Reactivation of spent FCC catalyst by mixed acid leaching for efficient catalytic cracking. *Journal of Industrial and Engineering Chemistry*, *92*, 236–242. https://doi.org/10.1016/j.jiec.2020.09.011
21. Maceiras, R., Alfonsín, V., Morales, F. J. (2017). Recycling of waste engine oil for diesel production. *Waste Management*, *60*, 351–356. https://doi.org/10.1016/j.wasman.2016.08.009
22. Mishra, A., Siddiqi, H., Kumari, U., Behera, I. D., Mukherjee, S., Meikap, B. C. (2021). Pyrolysis of waste lubricating oil/waste motor oil to generate high-grade fuel oil: A comprehensive review. *Renewable and Sustainable Energy Reviews*, *150*(January), 111446. https://doi.org/10.1016/j.rser.2021.111446
23. Moses, K. K., Aliyu, A., Hamza, A., Mohammed-Dabo, I. A. (2023). Recycling of waste lubricating oil: A review of the recycling technologies with a focus on catalytic cracking, techno-economic and life cycle assessments. *Journal of Environmental Chemical Engineering*, *11*(6), 111273. https://doi.org/10.1016/j.jece.2023.111273
24. Musadi, M. R., Salma, S., Rozada, F., Annisaa, N. R., Lucyana, A., Faulina, F., Khalid, F. (2024). Investigation of the Effects of Temperature and Catalyst on the Liquid Products of Waste Lubricant Oil Catalytic Pyrolysis. *E3S Web of Conferences*, *484*. https://doi.org/10.1051/e3sconf/202448401001

25. Muzayanah, I. F. U., Lean, H. H., Hartono, D., Indraswari, K. D., Partama, R. (2022). Population density and energy consumption: A study in Indonesian provinces. *Heliyon*, *8*(9), e10634. https://doi.org/10.1016/j.heliyon.2022.e10634
26. Nasim, M. N., Pervez, M. S., Yarasu, R. B., Lotia, N. V. (2014). Recycling waste automotive engine oil as alternative fuel for diesel engine : A Review. *Journal of Mechanical and Civil Engineering (IOSR-JMCE)*, *2014*, 46–50.
27. Naz, A., Ullah, M., Ali, S. D., Mahmood, T. (2014). *Nano Catalytic Conversion of Used Lubricating Oil into Diesel Fuel Nano Catalytic Conversion of used Lubricating Oil into Diesel Fuel*. *3*(January), 438–446.
28. Nowak, P., Kucharska, K., Kamiński, M. (2019). Ecological and health effects of lubricant oils emitted into the environment. *International Journal of Environmental Research and Public Health*, *16*(16), 1–13. https://doi.org/10.3390/ijerph16163002
29. Pan, Y., Shen, X., Yao, L., Bentalib, A., Peng, Z. (2018). Active sites in heterogeneous catalytic reaction on metal and metal oxide: Theory and practice. *Catalysts*, *8*(10). https://doi.org/10.3390/catal8100478
30. Parapat, R. Y., Laksono, A. T., Fauzi, R. I., Maulani, Y., Haryanto, F., Noviyanto, A., Schwarze, M., Schomäcker, R. (2024). Effect of design parameters in nanocatalyst synthesis on pyrolysis for producing diesel-like fuel from waste lubricating oil. *Nanoscale*, *16*(33), 15568–15584. https://doi.org/10.1039/d4nr01183j
31. Pereira, L. G. G., Yuan, Q., Heeres, H. J., Lima, S. B., Pires, C. A. M. (2024). Catalytic hydrotreatment of fast pyrolysis oils using Ni-Cu/Al-MCM-41 catalysts. *Journal of Analytical and Applied Pyrolysis*, *181*(June), 106593. https://doi.org/10.1016/j.jaap.2024.106593
32. Santhoshkumar, A., Ramanathan, A. (2020). Recycling of waste engine oil through pyrolysis process for the production of diesel like fuel and its uses in diesel engine. *Energy*, *197*, 117240. https://doi.org/10.1016/j.energy.2020.117240
33. Sinağ, A., Gülbay, S., Uskan, B., Uçar, S., Özgürler, S. B. (2010). Production and characterization of pyrolytic oils by pyrolysis of waste machinery oil. *Journal of Hazardous Materials*, *173*(1–3), 420–426. https://doi.org/10.1016/j.jhazmat.2009.08.100
34. Singh, V. K., Chatterjee, A., Maiti, P., Parmar, P., Mukherjee, S., Meikap, B. C. (2025). Pyrolysis of used lubricating oil using industrial waste-based catalyst for energy efficient fuel generation: A comprehensive review. *Fuel*, *391*(January), 134751. https://doi.org/10.1016/j.fuel.2025.134751
35. Song, X., Li, S., Li, K., Ning, P., Wang, C., Sun, X., Wang, Y. (2018). Preparation of Cu-Fe composite metal oxide loaded SBA-15 and its capacity for simultaneous catalytic oxidation of hydrogen sulfide and phosphine. *Microporous and Mesoporous Materials*, *259*(May 2017), 89–98. https://doi.org/10.1016/j.micromeso.2017.10.004
36. Sousa-Aguiar, E. F., Trigueiro, F. E., Zotin, F. M. Z. (2013). The role of rare earth elements in zeolites and cracking catalysts. *Catalysis Today*, *218–219*, 115–122. https://doi.org/10.1016/j.cattod.2013.06.021
37. Sousa, F. P., Silva, L. N., de Rezende, D. B., de Oliveira, L. C. A., Pasa, V. M. D. (2018). Simultaneous deoxygenation, cracking and isomerization of palm kernel oil and palm olein over beta zeolite to produce biogasoline, green diesel and biojet-fuel. *Fuel*, *223*(March), 149–156. https://doi.org/10.1016/j.fuel.2018.03.020
38. Zang, J., Yu, H., Liu, G., Hong, M., Liu, J., Chen, T. (2023). Research progress on modifications of Zeolite Y for improved catalytic properties. *Inorganics*, *11*(1). https://doi.org/10.3390/inorganics11010022